RSC Advances

PAPER

View Article Online
View Journal | View Issue



Cite this: *RSC Adv.*, 2026, **16**, 22048

# Systematic investigation on the segregation behavior of non-metallic atoms and their synergistic regulation mechanism of the hydrogen embrittlement at uranium grain boundaries

Longxian Li, Min Zhu,* Yan Li,* Chengxuan Peng, Longfei Pu and Zijian Wang

As a core fuel material for nuclear reactors, the segregation of non-metallic impurities and the hydrogen embrittlement effect at the grain boundaries of metallic uranium pose a serious threat to the long-term service safety of fuel elements. In this study, density functional theory (DFT) was employed to systematically compare the segregation behaviors of six typical non-metallic atoms (C, N, O, Si, P, and S) at uranium grain boundaries and reveal their synergistic regulatory mechanisms on grain boundary strength and hydrogen embrittlement. The key findings are as follows: all non-metallic elements exhibit an intrinsic tendency to segregate spontaneously at grain boundaries; the closer the site is to the grain boundary core, the stronger the segregation tendency and the more stable the binding state. Non-metallic elements weaken grain boundaries, with Si, P, and S inducing a significantly more pronounced weakening effect than C, N, and O. This difference is primarily attributed to the size-mismatch strain caused by the disparity in atomic radius between non-metallic dopants and the uranium matrix. The dominant mechanism underlying the synergistic grain boundary weakening by hydrogen and non-metallic elements is the chemical contribution: the weak bonds formed between hydrogen and non-metallic atoms replace the original strong non-metal-U bonds, resulting in a significant reduction in electron cloud density at grain boundaries. This study clarifies the non-metallic segregation at uranium grain boundaries and its influence on hydrogen behavior at the atomic scale, providing a key theoretical basis for the design of uranium-based fuels with enhanced resistance to hydrogen embrittlement.

Received 11th February 2026
Accepted 26th March 2026

DOI: 10.1039/d6ra01229a

rsc.li/rsc-advances



## 1 Introduction

Uranium is an important nuclear fuel and a component material with high chemical reactivity.[1,2] During usage, it readily reacts with environmental media, such as water, oxygen, and hydrogen, causing corrosion damage.[3,4] Hydrogenated corrosion is characterized by a fast corrosion rate, significant degradation of the surface state and mechanical properties, and severe harm to uranium materials. Grain boundaries, as common defects and fast diffusion channels in materials, are the main sites for hydrogen segregation and embrittlement. Additionally, during preparation and processing, metallic uranium inevitably incorporates trace levels of non-metallic impurity atoms (*e.g.*, C, N, O, Si, P, and S). Driven by thermodynamics, these impurity atoms also tend to segregate at the grain boundaries. This segregation not only directly alters the grain boundary structure but also interacts in a complex manner with hydrogen, thereby significantly affecting the segregation behavior and embrittlement effect of hydrogen. Therefore, revealing the segregation behavior of non-metallic atoms at grain boundaries and their nature of interaction with hydrogen is a key factor for understanding the microscopic mechanism of uranium hydrogen corrosion and developing strategies for anti-hydrogen embrittlement control.

Studies on the grain boundary structure of uranium and hydrogen behavior have shown that experimental research on uranium corrosion[5–9] generally confirms the grain boundaries as the preferred sites for hydrogen corrosion. Theoretically, we used first-principles calculations to reveal that typical uranium grain boundaries have a significantly higher hydrogen capture capacity than the bulk phase. Hydrogen atoms tend to diffuse within grain boundaries and rarely diffuse from grain boundaries into the bulk phase. The reconstruction of local electronic states at the hydrogen atom grain boundaries weakens uranium–uranium metallic bonds, thereby undermining grain boundary strength.[10] Jin *et al.*[11] used the same method and found that hydrogen atom capture in the twin-boundary region stems from the s–d interaction between hydrogen and uranium atoms, which produces the hydrogen capture effect.

Researchers have also explored the role of non-metallic impurities in uranium systems. Kautz *et al.*[12] used scanning

*Naval University of Engineering, China. E-mail: 1708051048@nue.edu.cn; 1920192563@nue.edu.cn*

electron microscopy and atomic probe tomography to conduct an in-depth characterization of non-metallic inclusions in as-cast low-enriched uranium nuclear fuel plates. They found that inclusions mainly exist at grain boundaries, with C and O as the two main types of non-metallic inclusions (with various morphologies) and Si and H as common impurities. Shamir *et al.*[13] found through hydrogenation corrosion experiments that carbon impurities can promote hydride formation. Demint *et al.*[14] showed in their experimental study that trace silicon impurities can rapidly accelerate the hydrogenation rate of uranium; the mechanism involves the disruption of the uranium lattice by silicon atoms, significantly reducing the critical strain required for hydride formation. For theoretical research, Houao[15] used density functional theory to systematically study the interactions between O atoms and different crystal planes of α-U and γ-U. Wang *et al.*[16,17] revealed the distribution characteristics of hydrogen in biphasic uranium through dynamic Monte Carlo simulations.

Existing experimental and theoretical studies have explored the hydrogen embrittlement behavior of uranium and the effects of non-metallic impurities. However, most studies focus on the influence of single hydrogen or single non-metallic impurities, and the synergistic mechanism of non-metallic segregation and hydrogen behavior at grain boundaries still lacks a systematic microscopic understanding. In particular, key scientific issues—such as the segregation behavior of non-metallic atoms at uranium grain boundaries, the regulation of hydrogen segregation following non-metallic segregation, and the physical basis of grain boundary strength weakening induced by the hydrogen-non-metallic synergistic effect—have not been clearly elucidated.

Based on this, the present study systematically investigates the segregation behavior of six typical non-metallic atoms at uranium grain boundaries using density functional theory. We calculated segregation energy, grain boundary energy, and strengthening energy to characterize the effect of segregation on the properties of grain boundaries. By decomposing the mechanical and chemical contributions of strengthening energy, combined with density of states (DOS), Crystal Orbital Hamiltonian Population (COHP), and differential charge density analysis, we revealed the regulatory mechanism of non-metallic doping on bonding at grain boundaries. We further investigated the influence of non-metallic segregation on hydrogen segregation behavior. Through the analysis of strengthening energy, interaction energy, and bonding in hydrogen-non-metallic co-doping systems, we elucidated the chemical nature of the synergistic effect of hydrogen and non-metals in weakening the grain boundary strength. We verified the evolution law of grain boundary strength through first-principles tensile testing. The results of this study will provide an important theoretical basis for the anti-hydrogen embrittlement design and service-life prediction of uranium-based fuel materials.

## 2 Calculation methods

All the computational work in this study was performed using the Vienna *Ab initio* Simulation Package (VASP) based on first-principles calculations within the framework of density functional theory (DFT).[18,19] The exchange–correlation interactions between electrons were described by the Generalized Gradient Approximation (GGA-PBE) functional.[20–22] The interactions between ions and electrons were treated using the projector augmented-wave (PAW) method, with the plane-wave cutoff energy set to 500 eV. The *k*-point mesh sampling of the Brillouin zone was generated *via* the Monkhorst–Pack scheme. Specifically, a $9 \times 9 \times 9$ *k*-point grid was employed for unit cell optimization, while a $5 \times 3 \times 1$ *k*-point grid was adopted for the optimization of grain boundary models. During the structural relaxation process, the shape and volume of the unit cell were fixed, and all atomic positions were allowed to relax freely until the convergence criteria were satisfied: the total energy was converged to $10^{-4}$ eV per atom, and the maximum force acting on each atom was less than 0.02 eV $Å^{-1}$. Previous studies have demonstrated that the correlation effects of 5f electrons in metallic uranium are less pronounced compared to those in its oxides (*e.g.*, $UO_2$).[23] Therefore, neither spin–orbit coupling (SOC) nor strong electron correlation effects were considered in the present work.

In this work, the symmetric tilt grain boundary (STGB), a type frequently observed in experiments, was investigated. It is designated based on the coincidence site lattice (CSL) model,[24] namely the $\sum 3[110](\bar{1}11)$ grain boundary. The atomic structures of grain boundaries were generated using Aimsgb,[25] an open-source Python library dedicated to constructing periodic grain boundary configurations. For the $\sum 3[110](\bar{1}11)$ grain boundary, one unit cell was rotated by approximately 70.53° relative to the other around the [110] axis of symmetry, with the $(\bar{1}11)$ plane defined as the grain boundary plane. For the α-uranium metal, the minimal grain boundary structure constructed by Aimsgb, which contains a single unit cell, comprises 12 atoms for the $\sum 3[110](\bar{1}11)$ grain boundary. In this study, a supercell containing 48 atoms was adopted for the $\sum 3[110](\bar{1}11)$ grain boundary system. Specifically, a 24-atom supercell was first established using Aimsgb, in which each grain consists of two body-centered cubic (bcc) unit cells; subsequently, the 48-atom supercell used in the calculations was constructed as a $2 \times 1 \times 1$ supercell by extending two such 24-atom cells along the *x*-axis. Fig. 1 displays the schematic of the grain boundary model, where Site 1, Site 2, Site 3, and Site 4 represent the four typical doping sites for non-metallic atoms.

Grain boundary energy is defined as the difference between the total energy of the grain boundary model and the total energy of the bulk model, divided by the interface area of the grain boundary model. Grain boundaries can represent the stability of grain boundary structures, and the calculation formula is as follows:

$$\gamma[Y] = (E_{\mathrm{tot}}^{\mathrm{GB\text{-}Y}} - E_{\mathrm{tot}}^{\mathrm{bulk\text{-}Y}})/2 \times S, \quad (1)$$

where *Y* is the doped solute element, $E_{\mathrm{tot}}^{\mathrm{GB\text{-}Y}}$ is the energy of the doped grain boundary structure, $E_{\mathrm{tot}}^{\mathrm{bulk\text{-}Y}}$ is the energy of the uranium bulk doped supercell, and *S* is the interface area of the grain boundary. The lower the energy at the grain boundary

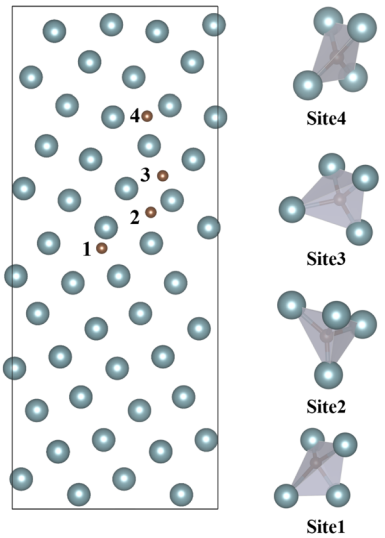


Fig. 1 Grain boundary model and doping sites.

interface, the stronger the bonding force between the two grains, indicating a more stable grain boundary structure.

To characterize the segregation tendency of non-metallic atoms, segregation energy was employed to quantify their segregation capability at the grain boundary, which is defined as the difference between the doping energy of non-metallic atoms at the grain boundary and that in the bulk lattice environment. The corresponding calculation formula is given as follows:

$$E_{\mathrm{seg}}^{\mathrm{GB}} = (E_{\mathrm{GB}}^{\mathrm{Y}} - E_{\mathrm{GB}}) - (E_{\mathrm{bulk}}^{\mathrm{Y}} - E_{\mathrm{bulk}}). \quad (2)$$

Its physical meaning is as follows: a negative segregation energy value indicates that non-metallic atoms tend to segregate preferentially at grain boundary sites. Conversely, a positive segregation energy value implies that these atoms are more inclined to stay in the bulk lattice environment.

Strengthening energy is used to characterize the effect of non-metallic atom doping on the grain boundary strength, and the corresponding calculation formula is given below:

$$E_{\mathrm{str}} = (E_{\mathrm{GB}}^{\mathrm{Y}} - E_{\mathrm{GB}}) - (E_{\mathrm{FS}}^{\mathrm{Y}} - E_{\mathrm{FS}}), \quad (3)$$

where $E_{\mathrm{FS}}^{\mathrm{X}}$ and $E_{\mathrm{FS}}$ refer to the total energy of solute atoms doped on the free surface and the complete free surface model, respectively. The more negative the strengthening energy, the more the doped solute atoms can enhance the bonding strength of grain boundaries. Similarly, when the strengthening energy is positive, it means that the doping of solute atoms will weaken the bonding strength of grain boundaries.

In the case of non-metallic atom-doped grain boundaries, the calculation formula for the segregation energy of hydrogen atoms at these grain boundaries is given as follows:

$$E_{\mathrm{seg}}^{\mathrm{H}} = (E_{\mathrm{GB}}^{\mathrm{H,Y,NU}} - E_{\mathrm{GB}}^{\mathrm{Y,NU}}) - (E_{\mathrm{bulk}}^{\mathrm{H,Y,NU}} - E_{\mathrm{bulk}}^{\mathrm{Y,NU}}), \quad (4)$$

where $E_{\mathrm{GB}}^{\mathrm{H,Y,NU}}$ and $E_{\mathrm{GB}}^{\mathrm{Y,NU}}$ represent the total energies of the non-metallic atom-doped grain boundary with hydrogen incorporation and without hydrogen, respectively. Correspondingly, $E_{\mathrm{bulk}}^{\mathrm{H,Y,NU}}$ and $E_{\mathrm{bulk}}^{\mathrm{Y,NU}}$ denote the total energies of the non-metallic atom-doped bulk lattice with hydrogen incorporation and without hydrogen, respectively.

When hydrogen atoms segregate at grain boundaries where non-metallic atoms have already segregated, interactions occur between hydrogen and non-metallic atoms. The calculation formula for their binding energy is given as follows:

$$E_{\mathrm{bind}}^{\mathrm{Y-H}} = (E_{\mathrm{GB}}^{\mathrm{H,Y,NU}} - E_{\mathrm{GB}}^{\mathrm{Y,NU}}) - (E_{\mathrm{GB}}^{\mathrm{H,NU}} - E_{\mathrm{GB}}^{\mathrm{NU}}), \quad (5)$$

where $E_{\mathrm{GB}}^{\mathrm{H,NU}}$ and $E_{\mathrm{GB}}^{\mathrm{NU}}$ represent the total energy of pure metal uranium grain boundary hydrogenation and hydrogen removal, respectively.

In the first-principles tensile test, the center of the grain boundary was designated as the initial fracture plane. The tensile process was simulated by continuously introducing an incremental separation distance to this fracture plane, with a step size of 0.5 Å per displacement. At each separation distance, the size and shape of the supercell were kept fixed, and the calculations were performed with the same computational precision and algorithm as those used for the grain boundary structural optimization.[26,27] During the tensile process, the energy change per unit area of the grain boundary, defined as the separation energy ($W_{\mathrm{sep}}{}^{x}$), is given by the following formula:

$$W_{\mathrm{sep}}{}^{x} = \frac{E(x) - E_0}{S_{\mathrm{GB}}}, \quad (6)$$

where $E(x)$ and $E_0$ represent the total energies of the tensile model at a separation distance of $x$ Å and 0.0 Å, respectively. The separation energy corresponding to the state where the grain boundary is completely fractured into two separate free surfaces is defined as the fracture energy ($W_{\mathrm{sep}}$). The Rose equation was employed to fit the separation energy data,[28] which is expressed as follows:

$$f(x) = W_{\mathrm{sep}} - \mathrm{W}_{\mathrm{sep}}(1 + x/\lambda)e^{(-x/\lambda)}, \quad (7)$$

where $\lambda$ is the feature separation distance. By taking the derivative of $f(x)$, the relationship between tensile stress and separation distance can be obtained as follows:

$$f'(x) = e^{(-x/\lambda)} W_{\mathrm{sep}} x/\lambda^2. \quad (8)$$

The maximum value of $f'(x)$, which is the theoretical tensile strength $\sigma_{\max}$, is obtained at a separation distance of $\lambda$ as follows

$$\sigma_{\max} = f'(\lambda) = W_{\mathrm{sep}}/(\lambda e). \quad (9)$$

# 3 Results and discussions

## 3.1 Segregation of non-metallic elements at the grain boundaries

Six typical and commonly observed non-metallic elements were selected for this study, including C, N, and O from the second

period, as well as Si, P, and S from the third period. First, we investigated the tendency for segregation of these non-metallic elements at the grain boundaries of metallic uranium and their corresponding effects on the grain boundary energy. Fig. 2 presents segregation energies and grain boundary energies of non-metallic elements at uranium grain boundaries. A negative segregation energy value indicates a preferential tendency for non-metallic elements to segregate at grain boundaries. As shown in the figure, segregation energies of C, N, O, Si, P, and S are all negative at the four doping sites, demonstrating that these elements possess an intrinsic thermodynamic tendency to segregate spontaneously at uranium grain boundaries. Kautz *et al.*[12] conducted an in-depth characterization of non-metallic inclusions in the as-cast low-enriched uranium fuel plates using scanning electron microscopy and atomic probe tomography techniques. They found that C and O inclusions mainly occurred in the grain boundary region, and Si was a common co-segregated impurity. This is consistent with our calculation that C, O, and Si have negative segregation energies. Overall, the absolute values of segregation energy exhibit a decreasing trend from Site 1 (closest to the grain boundary) to Site 4 (farthest from the grain boundary). This observation suggests that the closer a non-metallic element is to the grain boundary, the stronger its tendency to segregate and the more stable its binding state at the interface. The atomic arrangement at grain boundaries is loose and highly distorted, which can accommodate non-metallic elements of varying atomic sizes more effectively and release the associated strain energy. The grain boundary energy of the pure uranium grain boundary is 0.7 J $m^{-2}$. After doping with non-metallic elements, grain boundary energies at all four sites are lower than this value, indicating that doping with non-metallic elements enhances the stability of grain boundaries from an energetic perspective. The segregation energies and grain boundary energies of different non-metallic elements show an identical trend, which is attributed to the fact that both parameters are primarily determined by the energies of the doped grain boundary and bulk lattice systems. Among the selected elements, S exhibits the lowest segregation energy and the lowest grain boundary energy, whereas N has the highest values for both properties. Notably, both the segregation energy and grain boundary energy tend to decrease with the increasing atomic number of dopant elements. In summary, non-metallic elements C, N, O, Si, P, and S can segregate spontaneously at uranium grain boundaries and effectively reduce the grain boundary energy.

### 3.2 Mechanism of the influence of non-metallic elements on grain boundary strength

Based on the Rice–Wang grain boundary embrittlement model,[29] the effect of doped atoms on grain boundary strength can be quantified using strengthening energy. Among the four doping sites, Site 1 exhibits the lowest segregation energy for non-metallic elements; thus, strengthening energies of various elements at this specific site were calculated, as presented in Fig. 3. The strengthening energy can be decomposed into two components: mechanical contribution and chemical contribution.[30] Specifically, the mechanical contribution refers to the energy difference between the metallic uranium atomic structure before and after solute atom doping, and the sum of mechanical and chemical contributions equals the total strengthening energy. The calculated strengthening energies of all selected non-metallic elements at the grain boundary are positive, indicating that these elements all act to weaken grain boundaries. Among them, Si induces the most significant weakening effect, with a strengthening energy of 2.9 eV, and its large mechanical contribution is identified as the primary cause of grain boundary embrittlement. Demint *et al.*[14] found in their experiments that trace amounts of silicon impurities can rapidly accelerate the rate of uranium hydrogenation reaction. The mechanism they proposed is that silicon atoms disrupt the lattice structure of uranium, significantly reducing the critical strain required for hydride formation. This is highly consistent with the conclusion based on our calculations. The strengthening energies of S and P are the second highest after Si, with their mechanical contributions being comparable to each other. Notably, the chemical contribution of P exerts a grain boundary

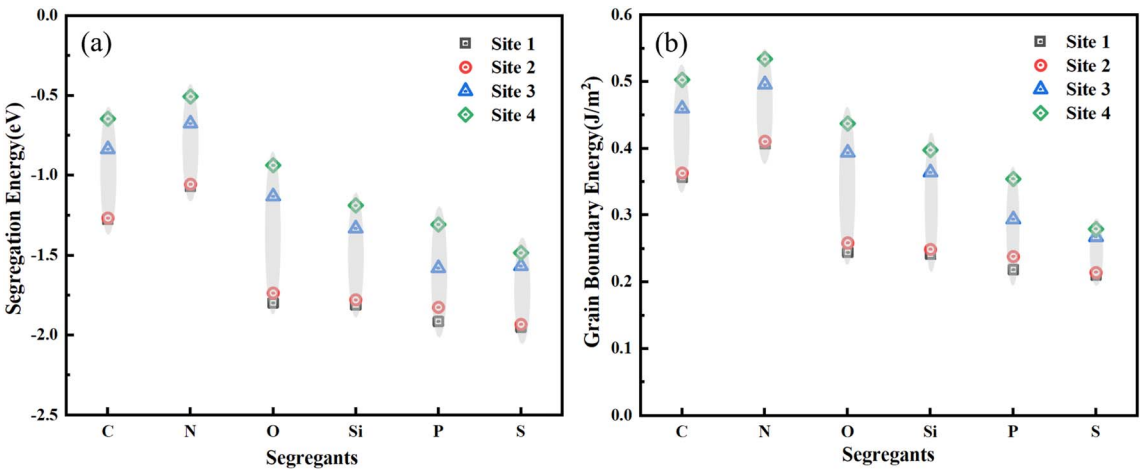


Fig. 2 Non-metallic elements in the uranium grain boundaries: (a) segregation energy and (b) grain boundary energy.

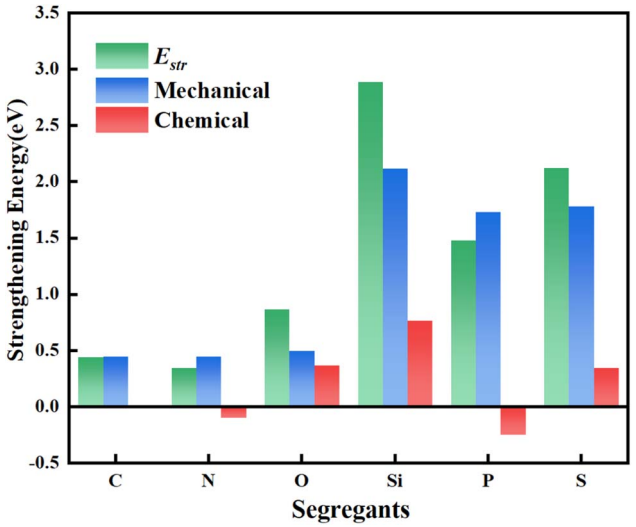


Fig. 3 Strengthening energy and mechanical and chemical contributions of the non-metallic elements.

strengthening effect, whereas that of S leads to grain boundary weakening. In contrast, grain boundary embrittlement effects induced by C, N, and O are relatively minor. The strengthening energy of C is almost entirely derived from its mechanical contribution. The mechanical contributions of N and O are quite similar; however, their chemical contributions differ distinctly: N has a chemical contribution of −0.1 eV, which enhances grain boundary strength, while O has a chemical contribution of 0.36 eV, which weakens the grain boundary.

In terms of the mechanical contribution, the values for C, N, and O are significantly lower than those for Si, P, and S. As can be seen from the atomic radii listed in Table 1, non-metallic elements with smaller atomic radii correspond to smaller mechanical contributions, while those with larger atomic radii give rise to larger mechanical contributions. This observation indicates that the mechanical contribution to strengthening energy is primarily derived from the size-mismatch strain induced by larger dopant atoms, which constitutes the main cause of grain boundary embrittlement related to strengthening energy. In contrast, chemical contributions vary among different elements, with both positive and negative values observed. This variation mainly originates from the bond strength between non-metallic atoms and metallic uranium atoms: a higher bond strength results in a negative chemical contribution, whereas a lower bond strength leads to a positive chemical contribution.

The density of states (DOS) can reflect the bonding characteristics between atoms. In this study, the partial density of states (PDOS) of the six selected non-metallic elements doped at grain boundaries of metallic uranium were calculated, as presented in Fig. 4. Near the Fermi level, the 5f orbitals of uranium atoms dominate with the highest peak intensity, while the d orbitals are distributed within the same energy range. The key distinction among the different non-metallic dopants lies primarily in the p orbitals of doped elements. Specifically, the p orbitals of O, Si, and S exhibit relatively weak intensity, and their PDOS peaks show no obvious hybridization with uranium orbitals, which corresponds to their chemical contribution to weakening the grain boundaries. For N, a distinct hybridization peak is observed in the energy range of −5.2 eV to −4.0 eV, which is mainly attributed to the strong hybridization between the p orbitals of N and the d orbitals of U, indicating a prominent bonding interaction. In addition, clear characteristic peaks are detected near −4.0 eV for C and near −4.5 eV for P, respectively. The chemical contribution of C is close to zero as its bonding strength is comparable to that of the U–U bond, leading to no significant tendency toward either strengthening or weakening the grain boundaries. Collectively, the C, N, and P elements provide strong chemical bonding reinforcement *via* their high-density p-electron states, which undergo intense hybridization with the d orbitals of uranium in the energy range of approximately −5.5 eV to −4.5 eV.

To quantitatively characterize the bonding strength between non-metallic atoms and metallic uranium at uranium grain boundaries, we calculated the Crystal Orbital Hamilton Population (COHP) of chemical bonds formed between non-metallic atoms and their nearest neighboring uranium atoms, as illustrated in Fig. 5. A positive COHP value represents bonding interactions, whereas a negative value indicates antibonding interactions. The wider the positive region of the curve below the Fermi level and the higher the peak intensity, the more fully the bonding orbitals are filled, signifying stronger bonding interactions. In the C-, N-, and P-doped systems, distinct and sharp negative COHP peaks are observed in the energy range from −5 eV to −2 eV below the Fermi level. This observation demonstrates intense orbital overlap between these non-metallic atoms and uranium, leading to the formation of strongly bonded states with high localization and low energy. Meanwhile, their antibonding states lie above the Fermi level and remain unoccupied by electrons, which constitutes the typical electronic structural feature of strong covalent bonds. In contrast, for the other three non-metallic elements (O, Si, and S), the negative COHP peaks corresponding to their bonding states are generally broader with lower peak intensities. In some of these systems, energy levels of the antibonding states are closer to the Fermi level or even partially occupied, which reduces the net bonding strength and results in overall weak bonding interactions. The Integrated Crystal Orbital Hamilton Population (ICOHP) value provides a quantitative measure of bond strength: the more negative the ICOHP value, the stronger the bonding interaction. The ICOHP of non-metallic bonds with uranium and hydrogen is shown in Table 2. Significant differences exist in the bonding strength between non-metallic atoms and uranium. Specifically, the C–U bond exhibits the most negative ICOHP value of −5.890 eV per bond, indicating the

Table 1 Atomic radii and electronegativities of the non-metallic elements

| Non-metallic elements | C | N | O | Si | P | S |
|---|---|---|---|---|---|---|
| Atomic radius (Å) | 0.77 | 0.70 | 0.66 | 1.17 | 1.10 | 1.04 |
| Electronegativity | 2.5 | 3.0 | 3.5 | 1.8 | 2.1 | 2.5 |

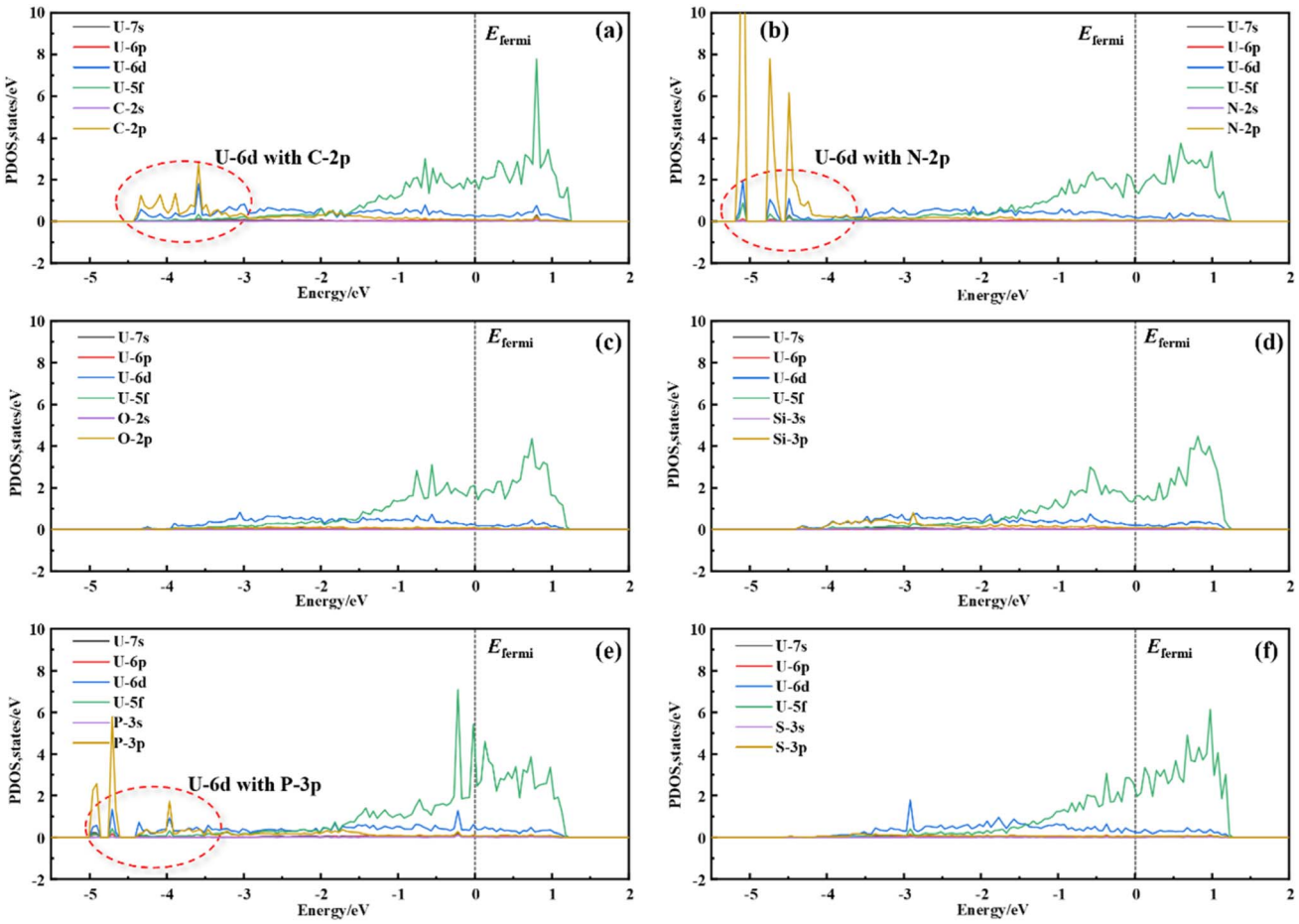


Fig. 4 Density of states plots of the uranium grain boundaries doped with non-metallic elements. Density of states doped with non-metallic elements: (a) C; (b) N; (c) O; (d) Si; (e) P; (f) S.

strongest covalent bonding interaction among all studied pairs. N–U and P–U bonds show the second-highest bonding strength, with their ICOHP values also falling in a highly negative range. The O–U bond has the least negative ICOHP value of −0.978 eV per bond, suggesting weak covalent character and low bond strength for this pair. Based on the absolute values of ICOHP, the bonding strength order for the six types of bonds is determined as follows: C–U > N–U > P–U > Si–U > S–U > O–U.

While previous sections have provided a static characterization of non-metallic element-doped grain boundaries, we further employed first-principles tensile tests to dynamically monitor the fracture process of these grain boundaries, as depicted in Fig. 6. In the separation distance range of 0–1 Å, atoms at the grain boundary were able to rearrange themselves, which partially offset the applied separation displacement and thus resulted in a slight variation in separation energy. As the separation distance increased further, the separation energy rose sharply; this stage can be analogized to the plastic deformation regime in mechanical tensile tests. Finally, when the separation distance reached 4–6 Å, the variation in separation energy gradually slowed down, and the separation energy approached its maximum limit, which is defined as the fracture energy. The relevant fracture parameters are summarized in Table 3. Among all the studied systems, the pure uranium grain boundary exhibited the highest fracture energy of 3.292 J $m^{-2}$. After doping with non-metallic elements, the fracture energy of grain boundaries decreased universally, with the S-doped system showing the lowest value of 2.325 J $m^{-2}$. This trend is consistent with the strengthening energy data reported earlier. The tensile stress was derived from fitting the separation energy data using the Rose equation. It first increased rapidly to a peak value and then decreased gradually, with the maximum tensile stress achieved at a separation distance of 1.5 Å. This trend is in good agreement with the variation tendency of the separation energy.

Fig. 7 depicts the bond length variations of specific uranium–uranium bonds during the tensile process for both undoped and non-metallic element-doped grain boundaries. Bond 1 refers to the bond length between U6 and U35, while Bond 2 denotes that between U19 and U30. Bond 1 represents the bond length variation of atoms on one side of the fracture plane. Initially, as the separation distance increases, the bond length increases progressively, corresponding to the elastic deformation stage. Typically, after reaching the maximum value at a separation distance of 1–2 Å, the length of Bond 1 begins to decrease. This phenomenon indicates that with the expansion

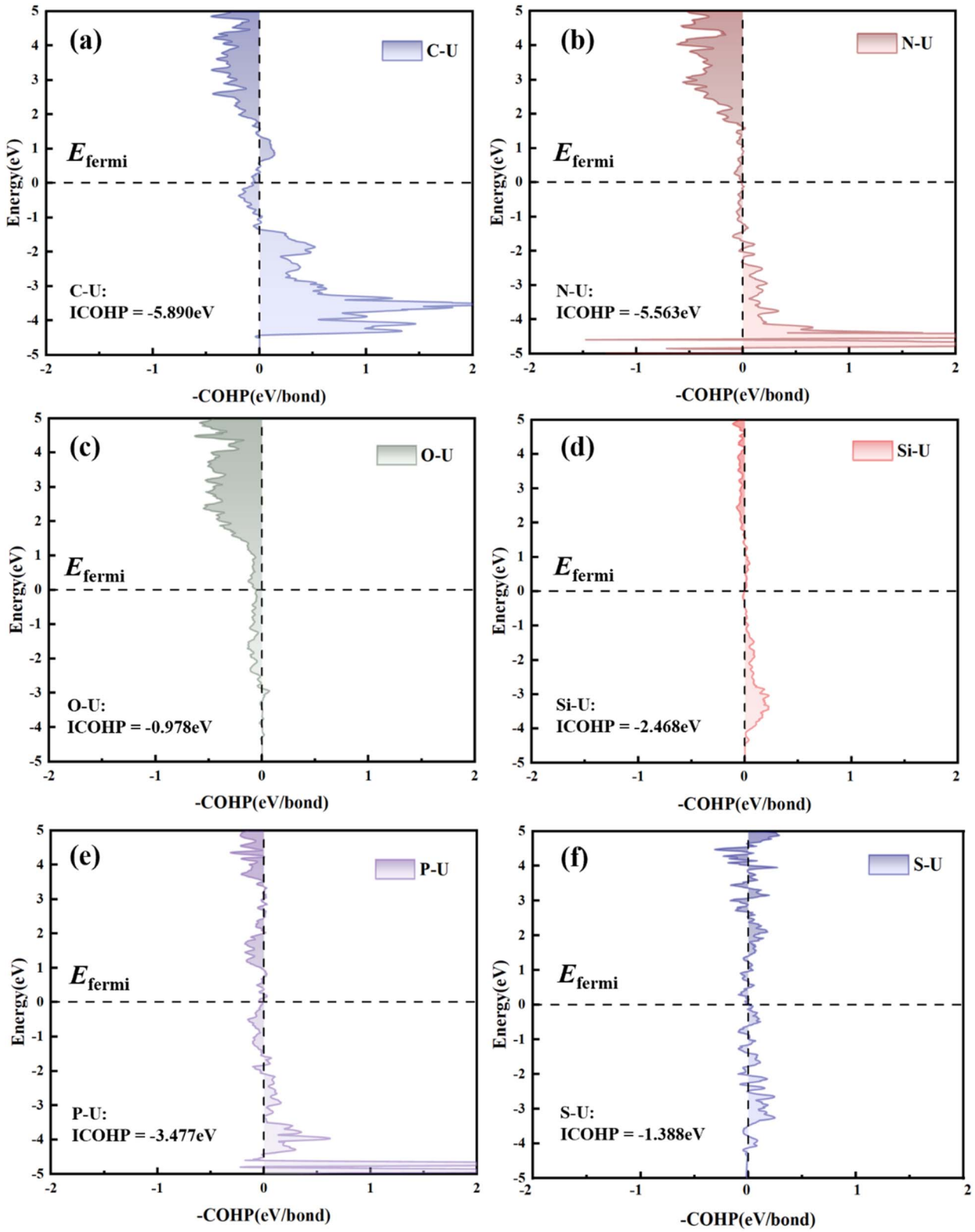


Fig. 5 (a) C–U, (b) N–U, (c) O–U, (d) Si–U, (e) P–U and (f) S–U bond COHPs in the grain boundaries.

of the fracture plane, interlayer atomic interactions weaken, allowing atoms in the lower layer to pull atoms on the fracture plane back toward the plane, which reduces the length of Bond 1 and eventually converges to a constant value of 2.55 Å. The uniform convergence of all Bond 1 lengths to the same value can be attributed to the fact that the lower layer beneath the

Table 2 ICOHPs of the non-metallic elements (unit: eV)

| Non-metallic elements | C | N | O | Si | P | S |
|---|---|---|---|---|---|---|
| Y–U | −5.890 | −5.563 | −0.978 | −2.468 | −3.477 | −1.388 |
| Y–H | −0.155 | −0.196 | −0.095 | −0.371 | −0.357 | −0.314 |
| H–U | −1.664 | −2.267 | −2.188 | −1.572 | −1.985 | −2.150 |

Table 3 Parameters related to the fracture of grain boundaries in first principles tensile testing

| System | Fracture energy ($J\ m^{-2}$) | Tensile strength (GPa) |
|---|---|---|
| Clean GB | 3.292 | 0.978 |
| C-doped GB | 3.023 | 0.864 |
| N-doped GB | 2.880 | 0.866 |
| O-doped GB | 2.805 | 0.808 |
| Si-doped GB | 3.167 | 0.952 |
| P-doped GB | 2.421 | 0.568 |
| S-doped GB | 2.325 | 0.560 |

fracture plane is a pure uranium surface, whereas doped non-metallic atoms are located on the upper surface. Moreover, at the initial stage of tension, the length of Bond 1 in doped systems is shorter than that in the pure uranium system, which is induced by the doping of non-metallic atoms. Bond 2 (between U19 and U30) is identified as the primary bond that ruptures during the grain boundary separation process. In the early stage of tension, the bond length undergoes relatively minor changes due to strong interatomic interactions. When the separation distance ranges from 1.5 Å to 2.5 Å, the lengths of Bond 2 in all non-metallic doped systems start to increase rapidly, marking the onset of the plastic deformation stage. Eventually, the interatomic interactions between the upper and lower layers diminish continuously, leading to a persistent elongation of the U–U bond length.

### 3.3 Synergistic effect of non-metallic atoms and hydrogen

To investigate the effect of non-metallic atom segregation on hydrogen segregation behavior, non-metallic atoms were first placed at Site 1, their optimal segregation site. Hydrogen atoms were then introduced to segregate within this grain boundary model, with a total of four segregation sites considered. These sites include Site 1*, the interstitial site closest to Site 1, as well as Sites 2 to 4, where the distance from the grain boundary increases progressively. The calculated segregation energies are presented in Fig. 8. For a given pre-segregated non-metallic element, the segregation energies at the four sites exhibit a regular distribution pattern: the segregation energy is the lowest at Site 1*, which is closest to the grain boundary. When hydrogen atoms are forced to occupy Site 1*, a site adjacent to this segregation trap, the system achieves the lowest energy state. As the distance from the grain boundary increases, the segregation energy rises gradually. This trend indicates that as the position moves away from the strong bonding region and strain field of the grain boundary core, the local atomic environment tends to resemble that of the bulk lattice, thus requiring higher additional energy to relocate hydrogen atoms to these sites. These results demonstrate that pre-segregated non-metallic atoms do not alter the fundamental segregation tendency of hydrogen atoms; instead, hydrogen atoms continue to co-segregate with non-metallic atoms at the grain boundary core. In the subsequent analysis, we focus on the scenario in which hydrogen atoms segregate at the grain boundary core.

As revealed by the above analysis, hydrogen atoms tend to co-segregate with non-metallic elements at the grain boundary core. The segregation and interaction energies of hydrogen atoms in non-metallic element-segregated grain boundaries were calculated, with the results presented in Fig. 9. The segregation energy of hydrogen atoms in the pristine grain boundary is −2.776 eV. After the segregation of C, N, and O atoms at the grain boundaries, the hydrogen segregation energy increases to 0.226 eV, 0.767 eV, and 1.023 eV, respectively. In contrast, the segregation of elements from the third period generally leads to a decrease in the hydrogen segregation energy. Specifically, the segregation energy of hydrogen shows negligible variation before and after Si doping, with a value of −0.142 eV. Following the doping of P and S atoms, the hydrogen segregation energy decreases further, which facilitates the

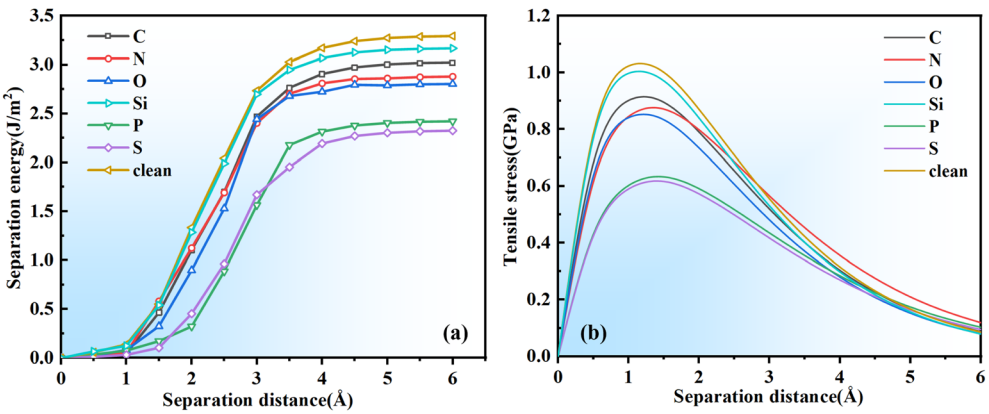


Fig. 6 Perfect grain boundaries and non-metallic element-doped grain boundaries: (a) separation energy and (b) tensile stress plots.

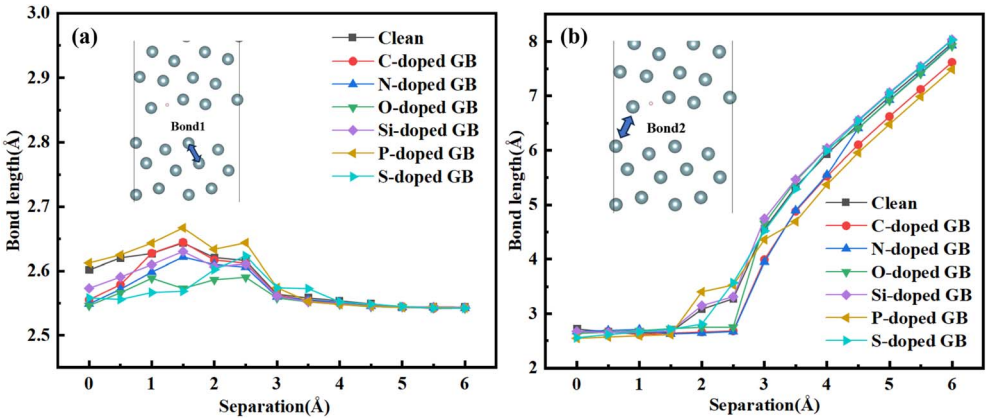


Fig. 7 Variation of bond length with the stretching distance in the grain boundary model during the stretching process for (a) U6–U35 and (b) U19–U30.

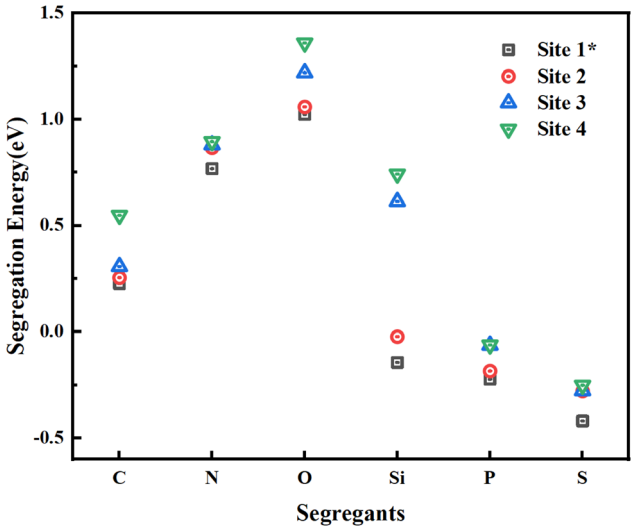


Fig. 8 Hydrogen segregation after the non-metallic doping.

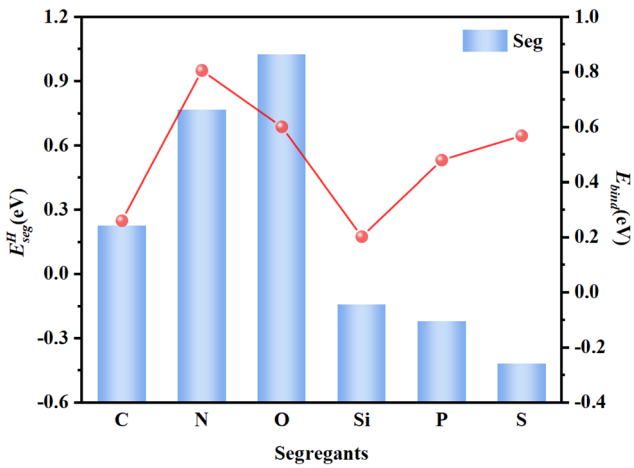


Fig. 9 Hydrogen segregation energy and interaction energy of the non-metallic element-doped grain boundaries.

segregation of hydrogen atoms at grain boundaries. The interaction energy quantifies the interaction intensity between hydrogen atoms and other non-metallic elements: a positive value indicates a repulsive interaction between hydrogen and dopant elements, while a negative value signifies an attractive interaction. Among the studied non-metallic elements, repulsive interactions are observed between each non-metallic element and hydrogen atoms. Notably, the repulsive effect of N atoms is the strongest, with an interaction energy of 0.805 eV, whereas Si atoms exhibit the weakest repulsive effect, corresponding to an interaction energy of 0.202 eV. In summary, repulsive interactions exist universally between non-metallic elements and hydrogen atoms, and doping of P and S elements can promote the segregation of hydrogen atoms at uranium grain boundaries.

In Fig. 10, blue bars represent the strengthening energies of metallic uranium grain boundaries doped with individual non-metallic atoms, orange bars denote the strengthening energy of uranium grain boundaries doped with individual hydrogen atoms, and gray bars indicate the increment in strengthening energy induced by the co-doping of hydrogen atoms with each non-metallic element. The total strengthening energy of the hydrogen-doped systems can be obtained by summing the values of the blue bars and the corresponding gray bars. The strengthening energy of a single hydrogen atom is 3.37 eV, which exerts the most severe embrittlement effect among the tested dopants. This finding confirms that hydrogen embrittlement is a critical factor responsible for the degradation of mechanical properties in uranium-based materials. After the introduction of hydrogen atoms into the non-metallic element-doped grain boundary systems, strengthening energies of these systems increase significantly, indicating a further exacerbation of the grain boundary embrittlement effect. The embrittlement potency of individual dopant atoms follows the order: Si > S > P > O > N > C. In contrast, the total embrittlement potency of co-doped systems (non-metallic elements plus hydrogen) follows the sequence: P > Si > S > O > N > C. This result demonstrates that hydrogen atoms exhibit the strongest synergistic effect with phosphorus atoms. In summary, non-metallic elements

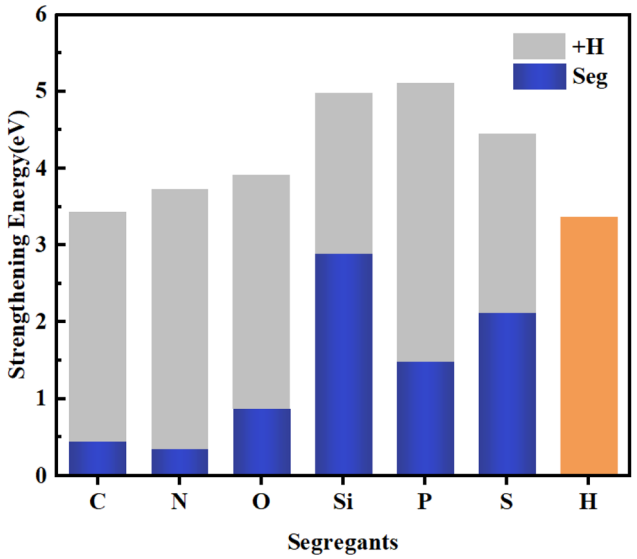


Fig. 10 Non-metallic elements and their hydrogen doping enhancement energy.

generally induce grain boundary embrittlement in uranium, with hydrogen exerting the most pronounced embrittlement effect. Moreover, hydrogen displays a synergistic and additive effect on the embrittlement behavior of other segregated elements; it can interact with these co-segregated elements to jointly exacerbate grain boundary embrittlement of uranium.

To explore the fundamental factors underlying the degradation of grain boundary strength induced by hydrogen atom doping, we calculated the mechanical and chemical contributions to grain boundary strength before and after hydrogen doping, with the results presented in Fig. 11. The mechanical contribution reflects the weakening effect on grain boundary strength caused by mechanical factors such as interatomic geometric matching and stress distribution. Prior to hydrogen doping, the mechanical contributions of C, N, and O to the weakening effect are relatively low, falling within the range of 0.4–0.5 eV. Among the studied elements, Si exhibits the highest mechanical contribution of 2.1 eV, followed by a slight decrease for P and S. These results indicate that in the absence of hydrogen, the mechanical effect of Si induces the most pronounced grain boundary weakening, whereas the mechanical weakening effects of other atoms are relatively insignificant. After hydrogen doping, mechanical weakening contributions corresponding to all segregated atoms increase by approximately 0.2–0.4 eV. This observation demonstrates that hydrogen doping enhances the grain boundary weakening effect induced by mechanical factors, though the overall increment remains relatively small. The chemical contribution characterizes the weakening effect on grain boundary strength arising from chemical factors, including interatomic chemical bonding and electronic interactions. In hydrogen-free systems, the chemical weakening contributions of C, N, O, P, and S are extremely low, being close to zero or even negative (a negative value indicates that the chemical effect enhances grain boundary strength). Only Si shows a moderate positive weakening contribution in the hydrogen-free state. These findings suggest that in the absence of hydrogen, chemical factors exert minimal influence on grain boundary strength and even produce a certain strengthening effect in some cases. In stark contrast, after hydrogen doping, chemical weakening contributions of all segregated atoms experience a substantial increase, which is far higher than those in the single-element doping state. This indicates that hydrogen doping transforms chemical factors into the dominant driver of grain boundary strength degradation, with the weakening magnitude far exceeding that induced by mechanical factors. In summary, the sharp surge in chemical contribution is the fundamental reason for hydrogen-doping-induced grain boundary weakening, which is closely related to the breakage of chemical bonds at grain boundaries and to the alteration of electronic interactions caused by the introduction of hydrogen atoms.

To uncover the chemical origin of the degradation of grain boundary strength induced by hydrogen doping, we calculated the Crystal Orbital Hamilton Population (COHP) and Integrated Crystal Orbital Hamilton Population (ICOHP) between hydrogen (H) atoms and non-metallic atoms segregated at grain

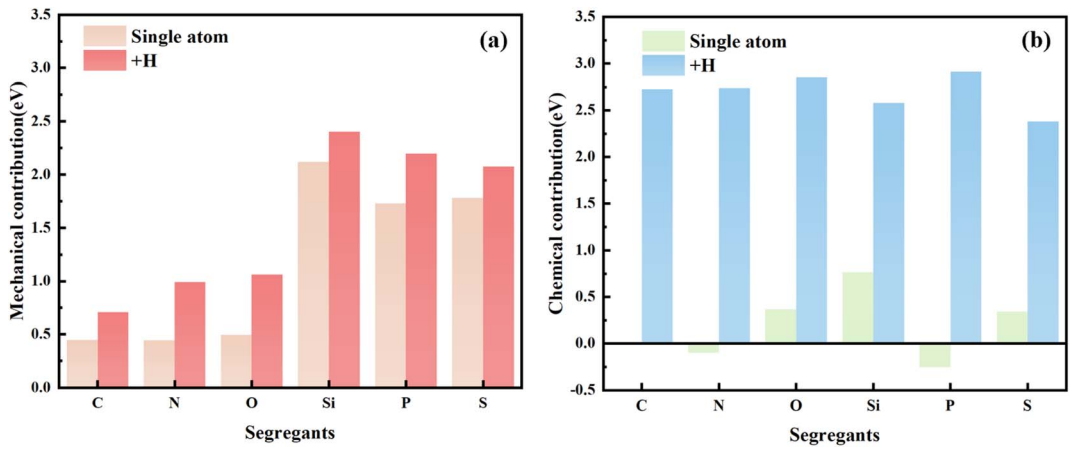


Fig. 11 (a) Mechanical and (b) chemical contributions of the non-metallic and hydrogen-doped materials.

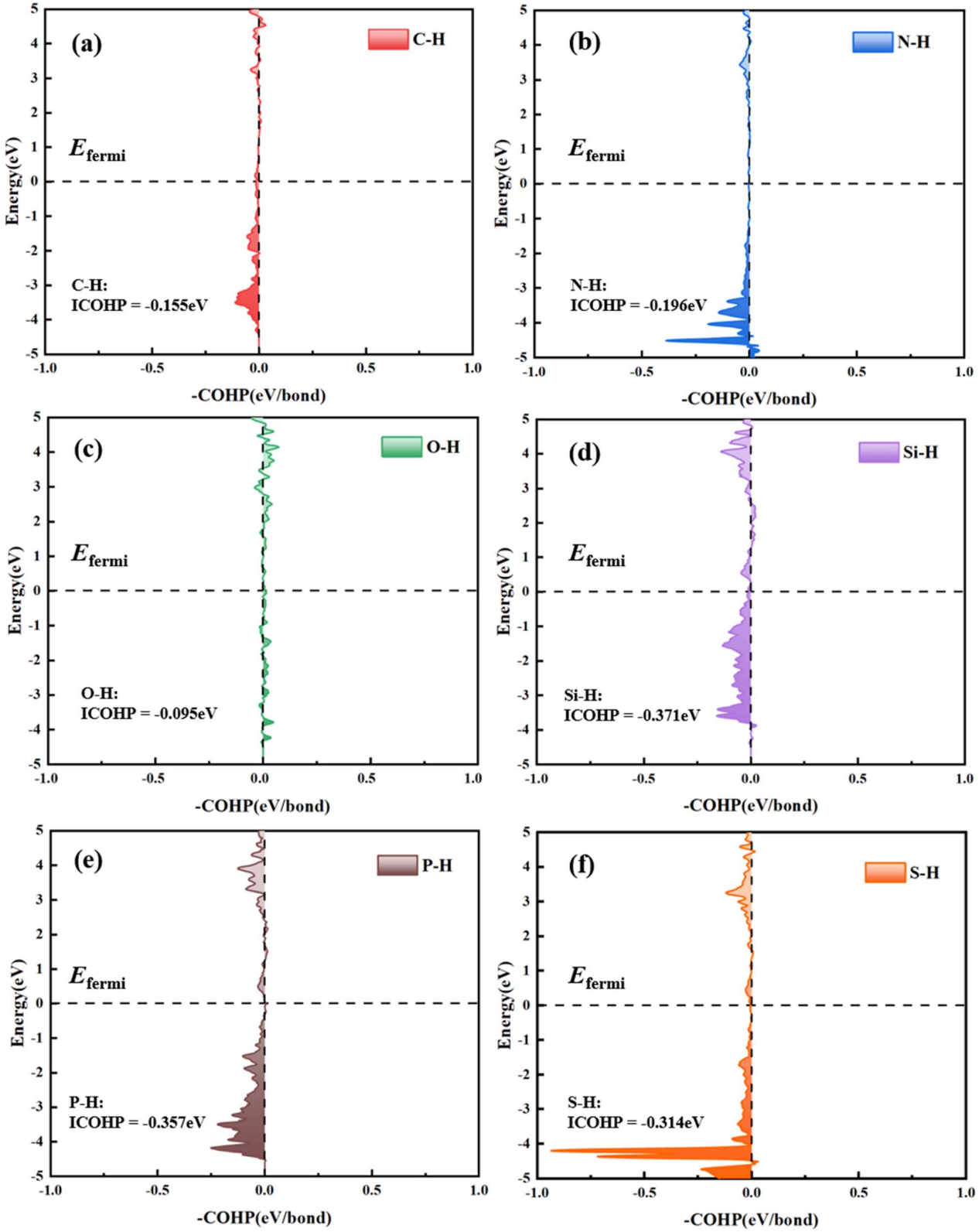


Fig. 12 (a) C–H, (b) N–H, (c) O–H, (d) Si–H, (e) P–H and (f) S–H bond COHPs in the grain boundaries.

boundaries. The results were then compared with the previously obtained bonding data for non-metallic atoms and uranium, as illustrated in Fig. 12. Integral analysis of COHP curves, namely ICOHP values, provides a direct quantitative measure of bonding strength. In this work, we found that the absolute ICOHP values of all H-non-metal bonds are far smaller than

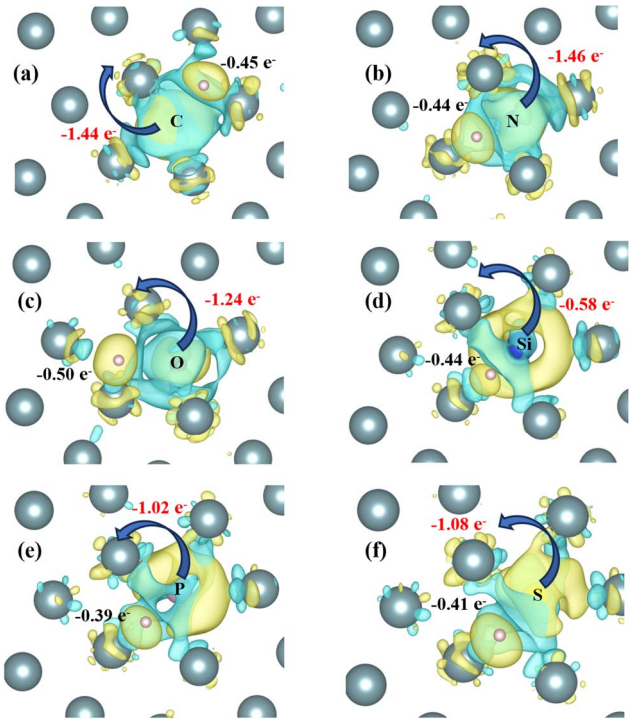


Fig. 13 Differential charge densities of the non-metallic atom-doped grain boundaries. Non-metallic doped GB differential charge density: (a) C; (b) N; (c) O; (d) Si; (e) P; (f) S.

those of the corresponding non-metal-U bonds. This result clearly confirms that, in the uranium grain boundary environment, the direct bonding strength between hydrogen atoms and non-metallic impurity atoms is significantly attenuated compared with that between non-metallic atoms and the uranium matrix. Below the Fermi level, in contrast to the sharp, deeply negative bonding-state peaks of Y–U bonds, most Y–H bonds are dominated by antibonding states. This observation stands in stark contrast to the characteristic feature of strong Y–U bonds, where the antibonding states are generally completely unoccupied. Collectively, the COHP analysis

Table 4 Parameters related to the fracture of grain boundaries in first principles tensile testing

| System | Fracture energy (J m$^{-2}$) | Tensile strength (GPa) |
|---|---|---|
| Clean GB | 3.098 | 0.960 |
| C-doped GB | 2.846 | 0.923 |
| N-doped GB | 2.821 | 0.929 |
| O-doped GB | 2.965 | 0.853 |
| Si-doped GB | 2.390 | 0.572 |
| P-doped GB | 2.250 | 0.555 |
| S-doped GB | 1.888 | 0.510 |

demonstrates that the direct chemical bonding strength formed between hydrogen atoms and non-metallic impurity atoms at uranium grain boundaries is much weaker than the bonding strength between the same non-metallic atoms and the uranium matrix.

To gain deep insights into the intrinsic nature of interactions between hydrogen atoms and non-metallic atoms at uranium grain boundaries from an electronic perspective, this study further calculated and analyzed the charge density difference and Bader charge of the H-non-metal bonding regions, with the results presented in Fig. 13. The values in red represent the number of electrons lost by non-metallic atoms, while the values in black denote the number of electrons lost by hydrogen atoms. This figure visually demonstrates charge redistribution during the bonding process, with yellow regions indicating electron accumulation and cyan regions representing electron depletion. In the current bonding environment, electrons do not flow unidirectionally from hydrogen atoms to the more electronegative non-metallic atoms. On the contrary, both hydrogen and non-metallic atoms donate electrons to the bonding region between them. The charge density maps show that the accumulated electrons (yellow regions) are mainly concentrated in the area slightly offset toward the non-metallic atom side along the central axis of the Y–H bond. This observation indicates that the Y–H bond exhibits distinct covalent bonding characteristics. In addition, across the studied

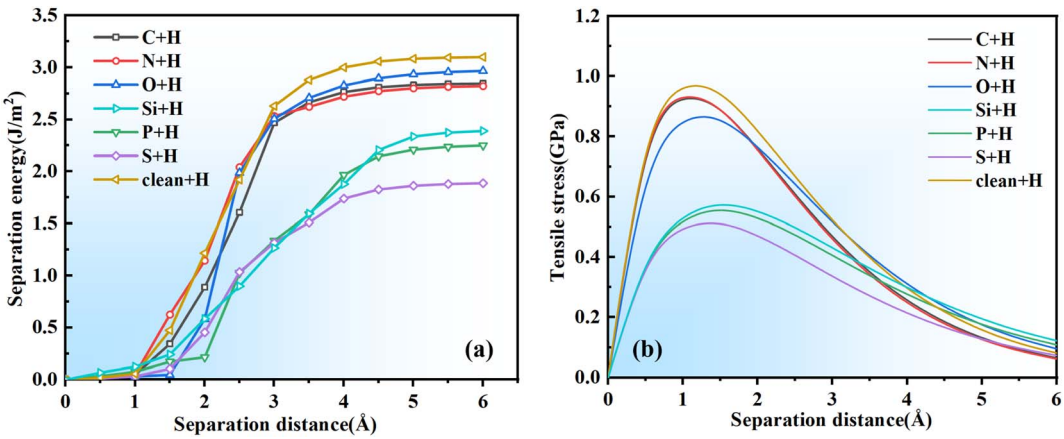


Fig. 14 Perfect grain boundaries and non-metallic hydrogenation doped grain boundaries (a) separation energy; (b) tensile stress.

systems, both non-metallic atoms (C, N, O, Si, P, S) and hydrogen atoms show electron loss characteristics (positive values for both red and black numbers), suggesting that electrons are transferred from these two types of atoms to the surrounding uranium atoms. In summary, after hydrogen doping, this specific electronic structure leads to an overall reduction in the electron cloud density of chemical bonds at grain boundaries. This finding directly corresponds to the chemical weakening mechanism revealed by the COHP analysis above—where strong non-metal-U bonds are replaced by weak H-non-metal bonds—thus explaining the fundamental origin of hydrogen-doping-induced grain boundary strength degradation from an electronic perspective.

We performed first-principles tensile tests on systems co-doped with non-metallic atoms and hydrogen. Fig. 14(a) and (b) depict the variations in separation energy and tensile stress with separation distance, respectively. The calculation results are shown in Table 4. The plateau value at the end of the separation energy curve corresponds to the fracture energy. As shown in the figures, both the fracture energy and maximum tensile stress of all non-metal-H co-doped systems are lower than those of the grain boundary with hydrogen atoms alone. Among these systems, the fracture energies of C-, N-, and O-doped systems are significantly higher than those of Si-, P-, and S-doped systems, which is consistent with the strengthening energy results reported earlier. A higher fracture energy corresponds to a larger maximum tensile stress, indicating that the strengthening energy parameter influences the mechanical properties at grain boundaries. Another noteworthy observation in Fig. 14(a) is that the separation energy curves of Si–H, P–H, and S–H co-doped systems exhibit an extended tensile stage. This phenomenon is mainly attributed to the fact that the atomic radii of Si, P, and S are larger than those of other elements, leading to a prolonged interatomic interaction stage during the tensile process. Despite this extended interaction period, the fracture energies of these three co-doped systems remain relatively low, which highlights the necessity of strictly controlling the doping levels of these three elements in uranium materials.

## 4 Conclusions

In this work, density functional theory (DFT) was employed to systematically elucidate the segregation behaviors of six typical non-metallic atoms at the uranium $\sum 3[110](\bar{1}11)$ grain boundary, as well as their regulatory mechanisms for hydrogen segregation, grain boundary bonding, and strength evolution. The main conclusions are summarized as follows:

All non-metallic elements exhibit an intrinsic tendency to segregate spontaneously at grain boundaries. The closer the site is to the grain boundary core, the stronger the segregation tendency and the more stable the binding state of dopant atoms. All non-metallic elements act to weaken uranium grain boundaries, with Si, P, and S inducing a much more significant weakening effect than C, N, and O. This distinction is primarily attributed to the size mismatch strain caused by the difference in atomic radii between non-metallic dopants and the uranium matrix. The bonding strength between non-metallic elements and uranium follows the sequence: C–U > N–U > P–U > Si–U > S–U > O–U.

The core mechanism underlying the synergistic grain boundary weakening effect induced by non-metallic elements and hydrogen is dominated by chemical contributions: the weak bonds formed between hydrogen and non-metallic atoms replace the original strong non-metal-U bonds at grain boundaries, leading to a significant reduction in the electron cloud density of interfacial chemical bonds. Further charge density difference analysis confirms that the electron loss of non-metallic atoms and the electron accumulation characteristics jointly weaken electronic interactions at grain boundaries, and this chemical weakening effect far outweighs the influence of mechanical contributions.

This study clarifies the regulatory effects of different non-metallic atoms on the stability of uranium grain boundaries and the behavior of hydrogen atoms and reveals the electronic structure origin of the synergistic grain boundary weakening effect caused by non-metal-H co-segregation. It provides a microscopic theoretical basis for optimizing the hydrogen embrittlement resistance of uranium-based fuels and thus reveals important guiding principles for the safe in-service performance of nuclear fuel elements.

Future research will focus on the actual service environment of reactors, systematically exploring the evolution of segregation behavior of non-metallic atoms under extreme conditions, as well as changes in the synergistic mechanism of hydrogen and non-metallic atoms; at the same time, by combining experimental characterization techniques, the applicability of theoretical models in complex environments is verified, further improving the theory of uranium based fuel grain boundary strengthening and anti-hydrogen embrittlement control, providing more comprehensive theoretical support for the long-term safe service of nuclear fuel elements.

## Conflicts of interest

There are no conflicts to declare.

## Data availability

The data for this article, including the grain boundary type, $\sum 3[110](\bar{1}11)$, are available at https://doi.org/10.1016/j.commatsci.2018.08.029.

## References

1 Q. G. Sheng, B. R. Cooper and S. P. Lim, First-principle study of hybridization effects and magnetic ordering in correlated-electron uranium systems, *Phys. Rev. B:Condens. Matter Mater. Phys.*, 1994, **50**(13), 9215–9225.
2 R. Springell, B. Detlefs, G. H. Lander, *et al.*, Elemental engineering: Epitaxial uranium thin films, *Phys. Rev. B:Condens. Matter Mater. Phys.*, 2008, **78**(19), 193403.
3 J. Petiau, G. Calas, D. Petitmaire, *et al.*, Delocalized versus localized unoccupied 5f states and the uranium site

structure in uranium oxides and glasses probed by x-ray-absorption near-edge structure, *Phys. Rev. B:Condens. Matter Mater. Phys.*, 1986, **34**(10), 7350–7361.

4 W.-D. Schneider and C. Laubschat, 5f-Electron Localization in Uranium Compounds, *Phys. Rev. Lett.*, 1981, **46**(15), 1023–1027.

5 M. Balooch and A. V. Hamza, Hydrogen and water vapor adsorption on and reaction with uranium, *J. Nucl. Mater.*, 1996, **230**(3), 259–270.

6 J. F. Bingert, R. J. Hanrahan, R. D. Field, *et al.*, Microtextural Investigation of Hydrided α-uranium, *J. Alloys Compd.*, 2004, **365**(1), 138–148.

7 T. Scott, G. Allen, I. Findlay, *et al.*, UD3 formation on uranium: Evidence for grain boundary precipitation, *Philos. Mag.*, 2007, **87**, 177–187.

8 C. P. Jones, T. B. Scott, J. R. Petherbridge, *et al.*, A surface science study of the initial stages of hydrogen corrosion on uranium metal and the role played by grain microstructure, *Solid State Ionics*, 2013, **231**, 81–86.

9 A. Banos and T. B. Scott, Statistical analysis of UH3 initiation using electron back-scattered diffraction (EBSD), *Solid State Ionics*, 2016, **296**, 137–145.

10 L. Li, M. Zhu, Y. Li, *et al.*, Atomic scale origin of hydrogen induced pitting corrosion in metallic uranium: first principles study of hydrogen behavior at uranium grain boundaries, *Int. J. Hydrogen Energy*, 2025, **159**, 150584.

11 J. Jin, Y. Zhang, W. Lv, *et al.*, The s-d interaction induced hydrogen trapping effect in α-U (130)/[001] twin boundary region, *Surf. Interfaces*, 2025, **61**, 106157.

12 E. J. Kautz, S. Shahrezaei, M. Athon, *et al.*, Evaluating the microstructure and origin of nonmetallic inclusions in as-cast U-10Mo fuel, *J. Nucl. Mater.*, 2021, **554**, 152949.

13 N. Shamir, Catalysis, by amorphous carbon, of H2 attack on oxidized U–0.1wt% Cr surfaces, *Appl. Surf. Sci.*, 2007, **253**(14), 5957–5960.

14 A. L. Demint and J. H. Leckey, Effect of silicon impurities and heat treatment on uranium hydriding rates, *J. Nucl. Mater.*, 2000, **281**(2), 208–212.

15 H. Liu, F. Liu, H. Zong, *et al.*, Initial oxidation behavior of α-U and γ-U surfaces, *J. Nucl. Mater.*, 2024, 592.

16 X.-X. Wang, H. Ji, Z. Li, *et al.*, What is the Role of Nb on Preferential Hydriding of Double-Phased Uranium, Stabilizing γ-U, or Avoiding Hydrogen Aggregation?, *J. Phys. Chem. C*, 2021, **125**(17), 9364–9370.

17 X.-X. Wang, Z. Li, B. Ao, *et al.*, A first-principles study on hydrogen distributions in theα-U/UO2interface, *J. Phys.: Condens. Matter*, 2020, **32**(19), 195002.

18 G. Kresse and D. Joubert, From ultrasoft pseudopotentials to the projector augmented-wave method, *Phys. Rev. B:Condens. Matter Mater. Phys.*, 1999, **59**(3), 1758–1775.

19 G. G. Kresse and J. J. Furthmüller, Efficient Iterative Schemes for Ab Initio Total-Energy Calculations Using a Plane-Wave Basis Set, *Phys. Rev. B:Condens. Matter Mater. Phys.*, 1996, **54**, 11169.

20 B. Dorado, M. Freyss and G. Martin, GGA+U study of the incorporation of iodine in uranium dioxide, *Eur. Phys. J. B*, 2009, **69**(2), 203–209.

21 M. Freyss, First-principles study of uranium carbide: Accommodation of point defects and of helium, xenon, and oxygen impurities, *Phys. Rev. B:Condens. Matter Mater. Phys.*, 2010, **81**(1), 014101.

22 X.-F. Tian, H. Wang, H. Xiao, *et al.*, Adsorption of water on UO2 (1 1 1) surface: Density functional theory calculations, *Comput. Mater. Sci.*, 2014, **91**, 364–371.

23 P. Söderlind, B. Sadigh, V. Lordi, *et al.*, Electron correlation and relativity of the 5f electrons in the U–Zr alloy system, *J. Nucl. Mater.*, 2014, **444**(1), 356–358.

24 T. Frolov, Q. Zhu, T. Oppelstrup, *et al.*, Structures and transitions in bcc tungsten grain boundaries and their role in the absorption of point defects, *Acta Mater.*, 2020, **159**(15), 123–134.

25 C. Jianli, L. Jian and Y. Kesong, Aimsgb: An algorithm and open-source python library to generate periodic grain boundary structures, *Computational Materials Science*, 2018, **155**, 92–103.

26 M. Černý, P. Šesták, P. Řehák, *et al.*, Ab initio tensile tests of grain boundaries in the fcc crystals of Ni and Co with segregated sp-impurities, *Mater. Sci. Eng., A*, 2016, **669**, 218–225.

27 P. Lazar and R. Podloucky, Cleavage fracture of a crystal: Density functional theory calculations based on a model which includes structural relaxations, *Phys. Rev. B:Condens. Matter Mater. Phys.*, 2008, **78**(10), 104114.

28 R. Janisch, N. Ahmed and A. Hartmaier, Ab initio tensile tests of Al bulk crystals and grain boundaries: Universality of mechanical behavior, *Phys. Rev. B:Condens. Matter Mater. Phys.*, 2010, **81**, 184108.

29 J. R. Rice and J.-S. Wang, Embrittlement of interfaces by solute segregation, *Mater. Sci. Eng., A*, 1989, **107**, 23–40.

30 V. I. Razumovskiy, S. V. Divinski and L. Romaner, Solute segregation in Cu: DFT vs. Experiment, *Acta Mater.*, 2018, **147**, 122–132.